HEAT DISSIPATION EFFECTS OF DIFFERENT NANOCOATED LATERAL FINS: AN EXPERIMENTAL INVESTIGATION

Premkumar MANI[1*], Santhanakrishnan RADHAKRISHNAN[2], Arulprakasajothi MAHALINGAM[3], Suresh VELLAIYAN[4]

[1]Department of Mechanical Engineering, Paavai Engineering College, Namakkal. Tamilnadu, India

[2]Department of Mechanical Engineering, SRM Institute of Science and Technology, Chennai, India

[3]Department of Mechanical Engineering, KCG College of Technology, Chennai, Tamil Nadu, India

[4]Department of Sustainable Engineering, Saveetha School of Engineering, Chennai, Tamil Nadu, India

[*] Corresponding authors; E-mail: premhnv@gmail.com (M. Premkumar)

Electrical batteries, mobile phones, central processing units of computing systems, and scientific instruments lose life due to improper heat transfer. Thermal management enables these electronics to run smoothly. This experiment measures heat sink temperature fluctuations during heating and cooling using lateral fins coated with graphene and carbon nanotubes. The study examined 15 W, 25 W, 35 W, and 45 W heat inputs to record the time to reach 40, 50, and 60 °C. Regardless of the coating material used in the heat sink, the time taken by the heat sinks to attain 60 °C was more than 3000 s. Heat input reduced the time to below 3000 s. Heat sinks dissipated heat until 32 °C during cooling. Infrared spectroscopy showed fins and heat sinks' energy retention. Convective heat transfer cooled the middle row of fins, and coated and uncoated heat sinks were evaluated for enhancement ratio. Coating the heat sink with graphene resulted in an enhancement in heat transfer by 1.15. While heating at 15 W, the CNT-coated heat sink exhibited a 1.9 enhancement ratio. The graphene-coated heat sink had an enhancement ratio for 25 W, 35 W, and 45 W heat inputs. The study found that operating temperature, input energy, and nano-coatings affect heat sink performance. This work can help optimise heat transfer from the heat sink to the atmosphere by determining nanocoating thickness. Mixed-material coating studies can disclose heat sink performance.

Keywords: Thermal management; heat sink; nano-coatings; graphene; carbon nanotubes; enhancement ratio

1. Introduction

Transferring heat efficiently is essential for the continued operation of both organic and inorganic systems, including but not limited to live organisms, industrial machinery, automobiles, electrical devices, and variable components. Heat is transferred via conduction and convection when the temperature difference between the heat source and the heat sink (the atmosphere) is small or moderate [1]. Components and devices are built with structural integrity and efficient heat dissipation

in mind. Proper heat transfer between the source and the washbasin can be ensured with the help of extended surfaces [2,3].

A wealth of research is devoted to the impact of extended surfaces on the functionality of components. Electronic components benefit from heat sinks because the air may circulate more freely over exposed surfaces. It is well known that the heat transfer rate through the heat sinks can be improved by employing active mechanisms such as cooling fans, heat storage mediums, and thermic fluids [4, 5]. Fans and clamping mechanisms enhance convenience but at the cost of increased device weight and, during fan operation, unwanted noise and vibration. Convective heat transfer occurs naturally in passive heat sinks [6, 7]. This approach is inferior to its active counterparts when transmitting high-quality heat energy. However, natural convection is more effective and efficient for facilitating the passage of low-grade heat energy in components maintained at relatively low temperatures [8, 9]. Smartphones, notebooks, desktops, televisions, unmanned aerial vehicles, closed-circuit television cameras, and wireless access points are remarkable devices. More than 80% of the power consumed by electronic devices is thought to be released as heat [10]. Proper thermal management is crucial to the operation and longevity of these electronic devices. Heat sinks provide for effective thermal management of electronic devices [11].

It has been noticed that increased surface area provided by an extended surface improves the heat sink's cooling performance. However, the heat transfer rate in the heat sinks is determined by parameters such as the fins' geometry, the fins' material properties, the fins' number of fins, the aspect ratio of the fins, and the capacity of the atmosphere to interact with the fins. According to experimental research by Jia *et al.* [12], the flow separation, disturbance effect, and mainline vortices made possible by the oval-shaped micro-pin fins improve heat transfer. Extending the fin tail and bringing it closer to the streamlining will limit the pump power to some level as the friction factor increases at first and increases again as the fin axial length ratio increases. Baig *et al.* [13] studied the thermal performance of slotted fin minichannel heat sinks for microprocessor cooling. They found that those with a fin spacing of 0.5 mm had a superior base temperature and thermal resistance than those with 1 mm and 1.5 mm fin spacings. In contrast to regular fin heat sinks, Jasim *et al.* [14] found that pin fin heat sinks with numerous circular stenosis on the fin surface had a poorer pressure drop and a higher heat transition. Their custom heat dispersants boost heat transfer by 100–223 percent compared to standard fins. Based on their experiments, Wang *et al.* [15] concluded that the gravity action could be partially neglected because the temperature distribution of the Light Emitting Diode (LED) array at different inclination angles was almost coincident and achieved good uniformity if the designed Over Head Projector (OHP) was operated at low filling ratios. It was also discovered that a high filling ratio can cause degradation of the lighting intensity of LED chips and that the temperature of the LED array is inversely related to the illumination intensity. For high-power LED cooling, the OHP design favoured a low % filling ratio of 30%. According to Ali *et al.* [16] experimental results, the most efficient pin-fin arrangement for heat transmission is a triangular one, with or without Phase Change Material (PCM). Mukeshkumar and Kumar [17] found that water, with the right fin height and thickness, significantly improved heat transfer in an electronic chip compared to air and motor oil.

Coating the enlarged surfaces, for instance, has been demonstrated to increase their effectiveness in heat management. After being nanocoated, the heat sink improved by 14% in its heating efficiency [18]. The cooling system's performance boost was proportional to the size of the heat sink (17% improvement; see also [10]). In a recent study, carbon nanotube-coated rectangular

brass fins were shown to increase heat transmission by an average of 12% compared to non-coated fin sinks, improved by 14% in their heating efficiency. The cooling system's performance boost was proportional to the size of the heat sink (17% improvement; see also [10]). In a recent study, carbon nanotube-coated rectangular brass fins increased heat transmission by an average of 12% compared to non-coated fins. Graphene coating of the heat storage media capsules boosted heat absorption by 6% in a heat sink, whereas carbon nanotubes (CNT) increased heat transfer by 11% [19]. The thermal conductivity of the heat sink was improved by 21.5 percent after being coated with graphene (0.1 vol. Pitting corrosion is minimised and component life is increased when aluminium heat sinks are covered [20, 21].

While there have been several investigations into heat sinks, none have used graphene and carbon nanotube (CNT) nanoparticle-coated lateral aluminium fins. Therefore, the present study aims to examine a heat sink equipped with aluminium fins along its sides. The dip coating technique applied the graphene and CNT coatings on the heat sink and the lateral fins [22]. The novelty of the work lies in estimating the heat dissipation effect on the aluminium heat sink provided with coating materials that function as the blackbody. Finding the heating and cooling cycles of heat sinks subjected to three distinct temperature limitations (40 °C, 50 °C, and 60 °C) is part of a thermal management study. Furthermore, the heat sinks were subjected to various operational conditions by being supplied with 15 W, 25 W, 35 W, and 45 W of heat, respectively. The findings were compared to those obtained using a non-coated heat sink.

2. Materials and methods

2.1. Design and fabrication of the heat sink

The processor unit of a desktop CPU was frequently becoming too hot due to the ineffectiveness of the active cooling mechanism. Designing a heat sink to enhance heat dissipation in central processing units of desktop computers solved the issue. CATIA V5 was used in the design of the heat sink. The heat sink's bottom was 80 mm by 75 mm in area and 10 mm thick. The top of the heat sink was equipped with six parallel lateral fins. The dimensions of each fin are 40mm by 5mm and 75mm in length, as shown in Fig. 1. The distance between the fins was set at 10 mm to improve atmospheric interaction. A three-axis vertical machining centre (VMC) milling machine can now utilise the converted IGES file of the planned heat sink.

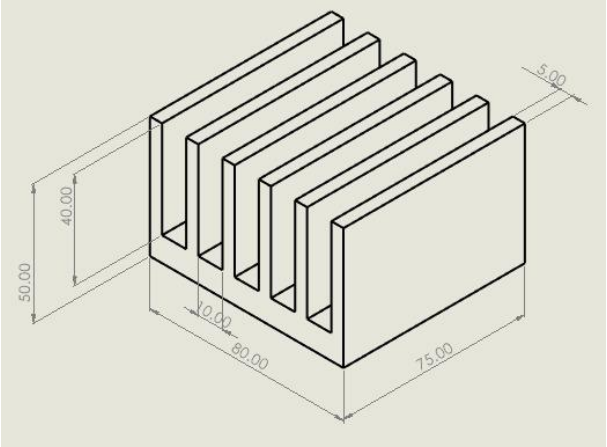

Figure 1. Heat sink dimensions

Table 1. Mechanical properties of AA6061

Property	Value	Unit
Tensile Strength	290	MPa
Vicker's Hardness	98	HV
Elongation	22	%
Density	2.7	g/cc
Impact strength	3.5	J
Melting temperature	585	^{o}C
Thermal conductivity	202	W/m.K
Coefficient of linear thermal expansion	$2.32*10^{-5}$	K^{-1}
Electrical conductivity	1.63	Ω/m

AA6061-T6 block measuring 85 mm x 80 mm x 60 mm was milled to create the heat sink. M/s Metal & Alloy Industries supplied the aluminium block in Chennai, Tamil Nadu, India. The characteristics of the aluminium alloy that was tested can be seen in Tab. 1. It can be observed that the chosen material for the heat sink exhibits low density, good strength and high thermal conductivity. The AA6061 block was securely fastened to the VMC machine's bed, with a base dimension of 85 mm by 80 mm. A 6-mm-diameter end mill cutter was used for the milling process. One of the heat sink's bottom sides had a blind hole drilled with a 6 mm diameter. The thermocouple utilised to gauge the heat sink's temperature was easily attached via the hole.

2.2. Nanocoating of the heat sink

Figure 2. Heat sinks: (a) CNT-coated, (b) Graphene-coated, and (c) non-coated

For the coating over the heat sink, we sourced the nanopowders of graphene (99.9% purity) and CNT (99.7% purity) from M/S Gogreen in Chennai, Tamil Nadu, India. Nanopowders of graphene had an average size of 350 nm, while CNTs averaged a diameter of 625 nm. Both the nanoparticles have lower thermal conductivity than the aluminium alloy AA6061. This makes it an excellent candidate to act as the insulation for the heat sink. Besides this, the colour of both the nanoparticles allows them to act as a black body. This allows excellent heat emission, a necessary characteristic of the heat sink. A controlled atmosphere (80 ^{o}C and 30% relative humidity) was used to dry the heat sink with lateral

fins before coating it. The coating was carried out using a dip coating technique. As part of this technique, the metal substrate, i.e., the AA6061-T6 heat sink, was cleaned by immersing it in boiling water for 30 minutes. The coating material was synthesised by mixing 0.5 wt—% of the nanoparticles in polyvinyl alcohol. Proper dispersal of the nanoparticles was ensured through ultrasonication for two h at room temperature, i.e., 30 ^{o}C. The substrate was dipped in the solution and maintained for 30 min. The coated heat sink was then treated using a muffle furnace. The heat treatment temperature was maintained at 200 ^{o}C for two h respectively. The coating thickness was measured using a coating thickness gauge with an integrated probe (Make: PosiTector, Mode: Standard). The coating thickness was found to be 25 µm. The heat sinks coated with nanoparticles and non-coated are shown in Fig.2.

2.3. Experimental investigation of the heat sinks

The test setup utilised to analyse the heat sinks' thermal management is seen in Figure 5. A 60-watt plate heater was employed in place of the electrical device to meet the demand for thermal energy. The plate heater took electrical energy as its input and produced thermal energy. Electric resistors regulate the input energy by limiting the voltage and current. Over the plate heater, we set up the heat sink's test module. The thermocouple (K type) was used to monitor the heat sinks for temperature variations. The thermocouples had a measurement error of 0.2 °C. The plate heater, heat sink, and thermocouple were housed in a see-through enclosure to conduct the heating and cooling cycles under regulated conditions. The data acquisition system included an Arduino UNOR3 module, a central processing unit, and a display unit, all linked to the thermocouple. The temperature reading was converted into a signal using the Arduino UNOR3 module. The central processing unit recorded the temperature readings to which the Arduino UNOR3 module was connected and shown on the screen. The study's assembled test setup is depicted in Fig. 3. The test apparatus was built to maintain a constant pressure environment around the fins during the experiment. This guarantees the fins can release their thermal energy into the surrounding air via convection.

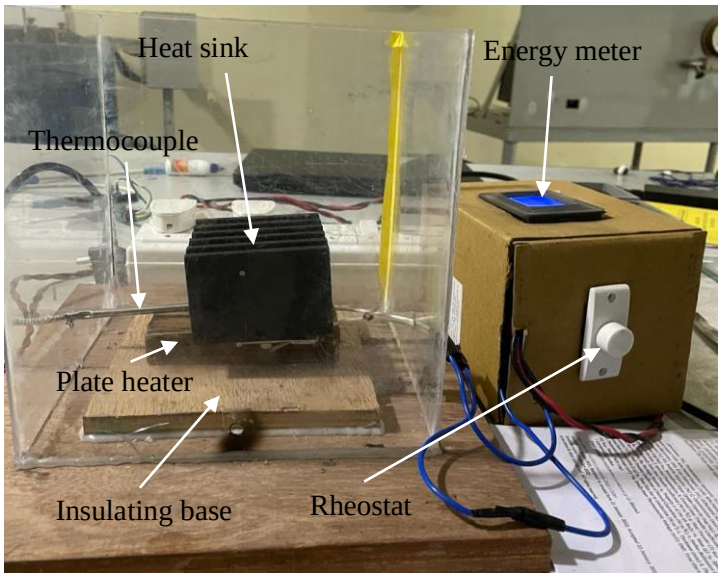

Figure 3. Photographic view of the assembled test rig

At 60-second intervals, the heat sink's temperature was monitored. Four different levels of heat input (15 W, 25 W, 35 W, and 45 W) were applied to the plate heater. Three distinct maximum temperatures, 40 ^{o}C, 50 ^{o}C, and 60 ^{o}C, were allowed to be reached while heating the heat sink. Inside,

the temperature was a comfortable 32 mm. Therefore, the pre-experiment temperature was 32 ^{o}C. Temperature swings were tracked as part of the heating cycle until the heat sink reached the target temperature. The plate heater was turned off at this time. After the temperature dropped, a log was kept to determine the heat sink's cooling cycle. The hot washbasin was allowed to cool until its temperature reached 32 ^{o}C. A thermal imaging camera (Make: Compact FLUKE pocket camera, Model: PTi120, 10800 pixels, Temperature range: -20 ^{o}C to 400 ^{o}C) was used to capture the infrared (IR) images from the heat sink. The thermal imaging camera had an error of 1.5 ^{o}C. Heat sinks with no coating, graphene coating, and carbon nanotube coating were used in the experiment. The resulting heat sink's enhancement ratio was calculated. The enhancement ratio was used to determine the extent to which the coated heat sinks improved performance.

2.4. Uncertainty analysis and numerical Study

Each heat sink in this study underwent the heating and cooling process five times. This research included an investigation of the degree of uncertainty involved. Measurements of the heating and cooling cycles allowed for the calculation of the total uncertainty ($T_{measure}$), which took into account both the equipment's (T_{eqp}) and the repetition of the uncertainty's (T_{rep}) uncertainty [23]. The statistical analysis of the measurement data eliminated the repetition uncertainty, and the device's precision within its measuring range explained the equipment uncertainty. The measurement error was calculated with Eq. (1).

$$T_{measure} = \sqrt{T_{rep}^2 + T_{eqp}^2} \quad (1)$$

Trep and Teqp were determined using Eq. (2) and Eq. (3), respectively.

$$T_{rep} = \frac{SD}{\sqrt{n}} \quad (2)$$

$$T_{eqp} = \frac{x}{\sqrt{n}} \quad (3)$$

where SD is the standard deviation, n is the number of repeated measurements, and x is the average accuracy of the thermocouple.

By comparing the highest temperature reached by the coated heat sink and the non-coated heat sink, an enhancement ratio was derived for the painted heat sink. Eq. (4) demonstrates this.

$$ER = \frac{T_c}{T_{nc}} \quad (4)$$

where ER is the enhancement ratio of the heat sink, T_c is the time taken to reach the maximum temperature of the coated heat sink, T_{nc} is the time taken to get the total temperature of the non-coated heat sink

3. Results and discussion

3.1. Influence of input energy on the heat sink

Figure 4 depicts the non-coated heat sink's response to varying input energies regarding temperature change. The heat sink was warmed using 15 W, 25 W, 35 W, and 45 W input energy. When the heat sink reached 32 ^{o}C, the experiment began. To determine the heating curve, the

temperature of the heat sink was monitored as it rose to a maximum of 60 ^{o}C. Then the power supply was suddenly turned off. The cooling curve was calculated by keeping track of the heat sink's temperature as it dropped. Time series analysis was used to compare heating and cooling curves. The temperature of the heat sink was shown to increase linearly in response to the supplied heat, and this trend was seen to hold across a wide range of input energies. The aluminium heat sink's superior capacity to dissipate heat explains the linear rise in thermal power. The temperature swing during 15 W of heating was skewed to the right. This shows that the low input energy resulted in a steady increase in the heat sink's temperature. However, a somewhat fast rise in heat sink temperature was seen as input energy increased. This suggests that the heat sink is heated rapidly in response to the increased input energy.

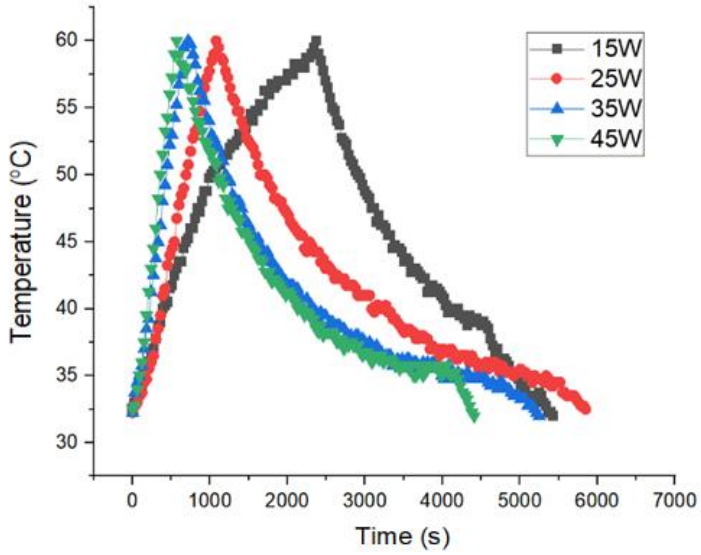

Figure 4. Heating and cooling curve of non-coated heat sink

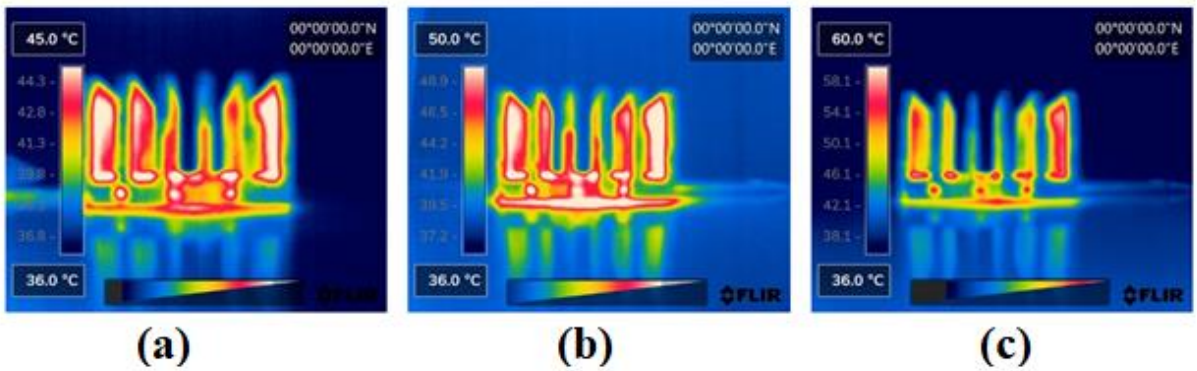

Figure 5. IR images at various temperatures on a non-coated heat sink: (a) 40 ^{o}C; (b) 50 ^{o}C; and (c) 60 ^{o}C

It was observed that the cooling curve deviated from a linear relationship between temperature and time after the input energy was turned off. The heat sink's cooling curve was recorded until its temperature reached 32 ^{o}C again. When the heat sink was being heated, there was a corresponding rise in the surrounding area's ambient temperature. The contained portion sustains heating, which causes a non-linear temperature change while the heat sink cools. Temperature variation in the enclosure can be

seen as a curve when the heat sink cools down. The section was rapidly heated at input powers more significant than 15 W. However, the enclosure was progressively heated when the input power was only 15 W. Because the cage was heated gradually, enough heat energy could be stored in the air within the enclosure. This meant the heat would continue to radiate even after the plate heater was turned off. The heat sink's temperature gradually dropped once the power was turned off. The same behaviour was seen when the input power was reduced to 25 W. However, when the input power was 35 W or 45 W, the heat sink cooled off quickly when the power was turned off. The extra heat energy absorbed during the procedure is responsible for this phenomenon.

Infrared (IR) images of a non-coated heat sink at 40 ^{o}C, 50 ^{o}C, and 60 ^{o}C are shown in Fig. 5. It has been discovered that the heat sink's base emits the most radiation, regardless of the temperature it reaches. Maximum heat energy was transferred via the fins directly above the plate heater as the temperature rose from the initial temperature to 40 °C. As can be seen in Fig. 5a, this led to a rise in the amount of energy emitted by these fins. Natural convection was also investigated in a vertical plate-fin heat sink. Increasing the fins' diameter by a factor of 10 increased their thermal resistance by 10 % in the experiment [24]. The environment in contact with the fins in the middle row must have been intensely warmed. The air's density dropped precipitously, sending the molecules spiralling upward and away from the fins. The middle row of fins benefited from enhanced convective heat transmission, resulting in a significant decrease in temperature.

When the heat sink was heated to 50 ^{o}C, comparable radiation emanated from the fins in infrared photos. However, It was found that the heat sink let forth more radiation. The heat sink's base and fins have reached their temperature limit, which explains this behaviour. As may be seen in Fig. 5b, the highest temperature reached 45 ^{o}C. To raise the temperature, the heat sink was continuously heated. It was discovered that the heat sink's base was the source of the most radiation. This occurred because the fins facilitated heat loss to the atmosphere via convection. As long as the plate heater was on, the heat sink's base was heated via conductive heat transfer, reaching an increasingly high temperature. Figure 5c displays the maximum temperature obtained during the experiment, which was 58 ^{o}C.

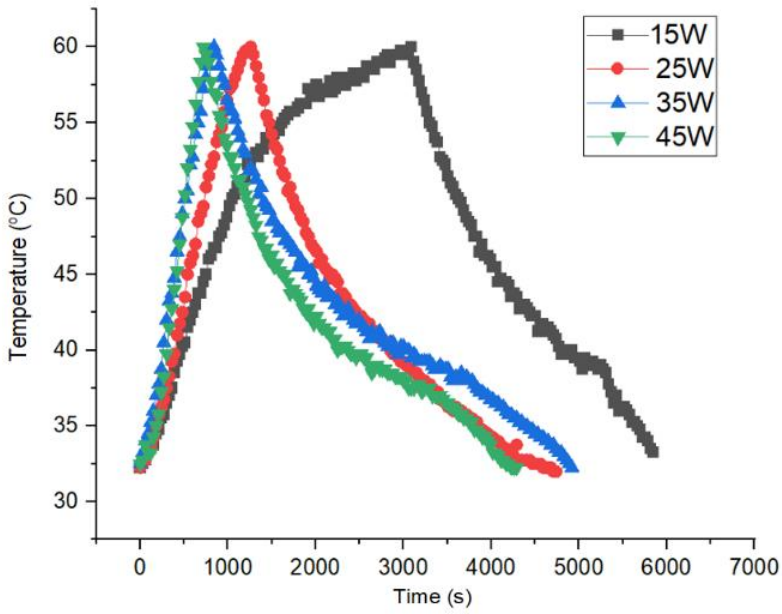

Figure 6. The heating and cooling curve of the graphene-coated heat sink

The graphene-coated heat sink's response to a change in input energy is depicted in Fig. 6. The heating curve followed the same pattern as the non-coated heat sink until the input power reached 15 W. However, the heating curve grew nonlinearly when 15 W of input energy was used. It is hypothesised that the graphene particles impeded the heat transfer efficiency between the heat sink and the atmosphere within the enclosure, leading to the gradual heating of the heat sink. The lengthened time required for the graphene-coated heat sink to achieve its maximum temperature of 60 ^{o}C indicates this. The efficiency of heat transmission between the heat sink and the atmosphere through the graphene coat increased as the input power was raised above 15 W. The cooling curve followed the same pattern as that of a heat sink that had not been covered.

Temperatures of 40 ^{o}C, 50 ^{o}C and 60 ^{o}C were used to capture infrared images of a heat sink coated with graphene (Fig. 7). Radiation from the heat sink was found to have increased after being coated with graphene. An increase in the heat sink's temperature is responsible for this effect. The graphene layer helped ensure that the heat was distributed evenly. The highest the heat sink got to was much above 50 ^{o}C. Graphene nanoparticles may have absorbed thermal energy from heating the heat sink. As seen in Fig. 7c, the heat sink reached a maximum temperature of 58 °C, which was maintained uniformly along the base and outer side rows of fins. Graphite and graphene were applied to an aluminium plate and then tested. The experiments showed that the heat transfer was enhanced by 11% due to the graphene covering [25].

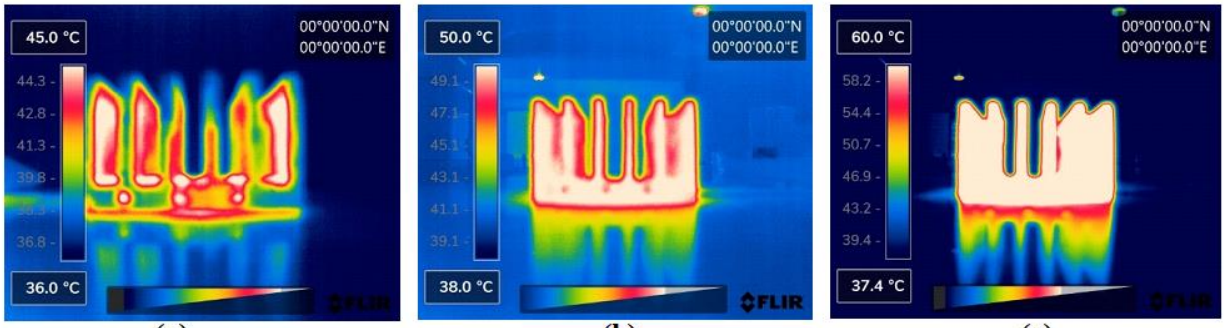

(a) (b) (c)

Figure 7. IR images at various temperatures on graphene-coated heat sink: (a) 40 ^{o}C; (b) 50 ^{o}C; and (c) 60 ^{o}C

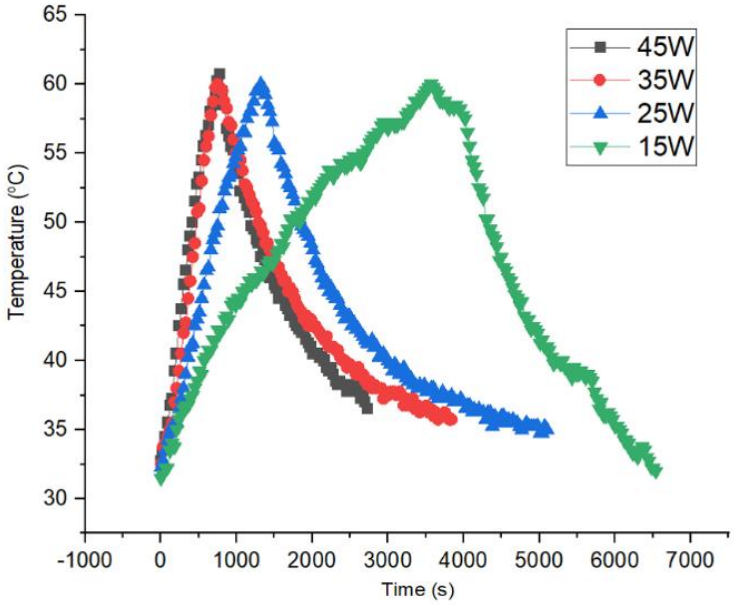

Figure 8. Heating and cooling curve of CNT-coated heat sink

Figure 8 depicts the CNT-coated heat sink's response to a change in input energy in terms of temperature. The heating curve followed the same pattern as the non-coated heat sink until the input power reached 15 W. However, the heating curve grew nonlinearly when 15 W of input energy was used. Inferred from this is that the CNT particles impeded heat transmission efficiency between the heat sink and the atmosphere within the enclosure, leading to the gradual heating of the heat sink. The CNT-coated heat sink takes longer to heat up to its maximum temperature of 60 ^{o}C, proving this. Coating the heat sink with CNT took around 4200 seconds longer to reach 60 ^{o}C than graphene. The efficiency of heat transmission from the heat sink to the atmosphere through the CNT coat increased as the input power increased to greater than 15 W. When the heat input was less than 45 W. However, the time needed to reach the maximum temperature rose. Compared to graphene, the CNT nanoparticles displayed less cooling in the trend cooling curve of the CNT-coated heat sink.

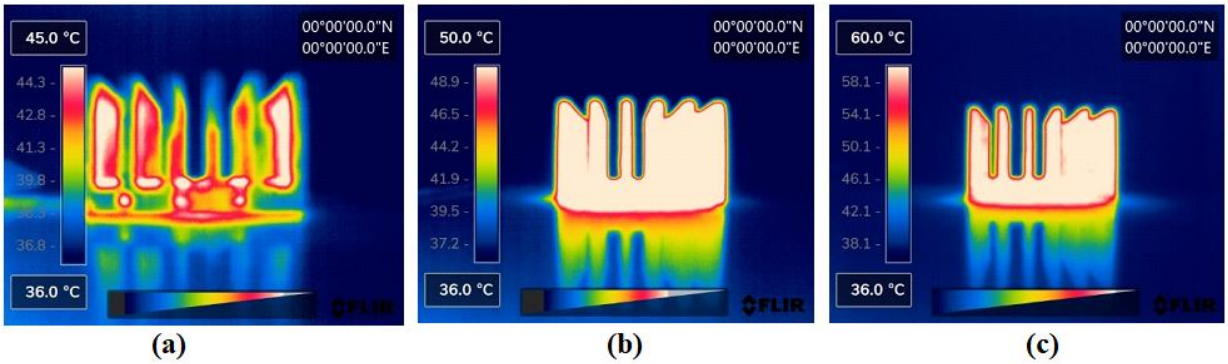

(a) **(b)** **(c)**

Figure 9. IR images at various temperatures on CNT coated heat sink: (a) 40 ^{o}C; (b) 50 ^{o}C; and (c) 60 ^{o}C

The infrared image of the CNT-coated heat sink is shown in Fig. 9 at several temperatures, including 40 ^{o}C, 50 ^{o}C, and 60 ^{o}C. After being coated with CNTs, the heat sink radiated more heat than before. An increase in the heat sink's temperature is responsible for this effect. The CNT coating ensured that the heat was dispersed evenly. Fig. 9a and Fig. 9b show that the radiation is uniform around the room, proving this point. In both instances, the heat sink's highest temperature exceeded 60

^{o}C. The term "heat sink " implies that the CNT nanoparticles absorbed heat energy. Maximum temperatures of more than 60 ^{C} were reached uniformly along the fins' base and outer side rows, as shown in Fig. 9c. An aluminium plate was coated with aluminium and silicon dioxide for an experiment. The thermal resistance decreased by 18% after coating [26, 27].

3.2. Time Taken During Heating of the Heat Sink

The time required for the uncoated heat sink to reach 40 ^{o}C, 50 ^{o}C, and 60 ^{o}C is displayed in Fig. 10. The heat sink was warmed using 15 W, 25 W, 35 W, and 45 W of input energy. The time needed to reach the maximum temperature was lengthened when the heat input was 15 W. In around 420 seconds, the heat sink warmed up to 40 ^{o}C. It took the heat sink about 1150 seconds to heat up to 50 °C. Similarly, it took the heat sink about 2100 s to heat up to 60 °C. These numbers are all in line with a 15 W heat source. The maximum temperatures of 40 ^{o}C, 50 ^{o}C, and 60 ^{o}C could be reached 31%, 56.5%, and 43.8% faster when the input energy was increased to 25 W. When the highest temperature was 60 ^{o}C, there was a significant drop in the temperature's variability. Adding more power to the heat sink is assumed to have increased the heat transfer rate via conduction. As a result of this event, heat energy was transferred to the aluminium heat sink rapidly. This phenomenon is explained by the shorter time it takes for the heat sink to reach its maximum temperature when subjected to heat inputs of 35 W and 45 W.

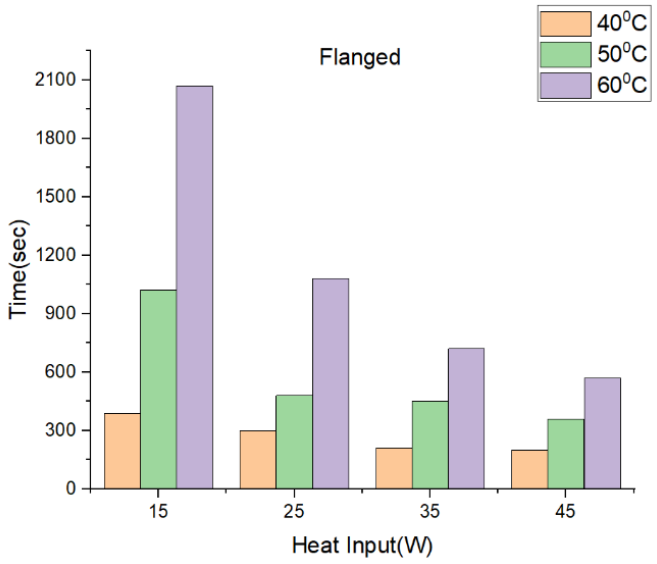

Figure 10. Time taken during heating of non-coated heat sink

The time required for a graphene-coated heat sink to reach 40 ^{o}C, 50 ^{o}C, and 60 ^{o}C is displayed in Fig. 11. The heat sink was warmed using 15 W, 25 W, 35 W, and 45 W of input energy. The time needed to reach the maximum temperature was lengthened when the heat input was 15 W. In about 490 seconds, the heat sink reached 40 ^{o}C. In about 1100 s, the heat sink reached 50 ^{o}C. Similarly, the heat sink heated to 60 ^{o}C in around 1890 seconds. These numbers are all in line with a 15 W heat source. Graphene coating the heat sink made it take longer to reach the three target temperatures than a non-coated heat sink. The presence of the graphene layer likely hindered the convection of air within the enclosure.

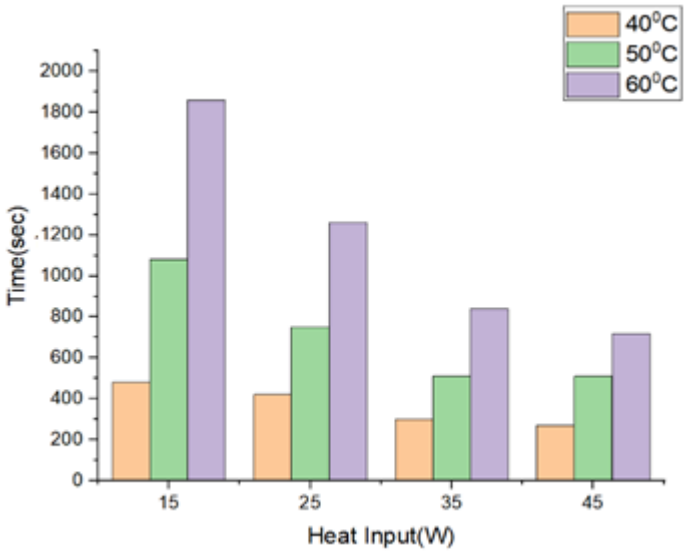

Figure 11. Time taken during heating of graphene-coated heat sink

The highest temperatures of 40 ^{o}C, 50 ^{o}C, and 60 ^{o}C were reached 14.3 percent, 31.8 percent, and 30.2 percent faster when the input energy was increased to 25 W. When the highest temperature went 60 °C, there was a significant drop in the temperature's variability. Adding more power to the heat sink is assumed to have increased the heat transfer rate via conduction. As a result of this event, heat energy was transferred to the aluminium heat sink rapidly. This phenomenon is explained by the shorter time it takes for the heat sink to reach its maximum temperature when subjected to heat inputs of 35 W and 45 W.

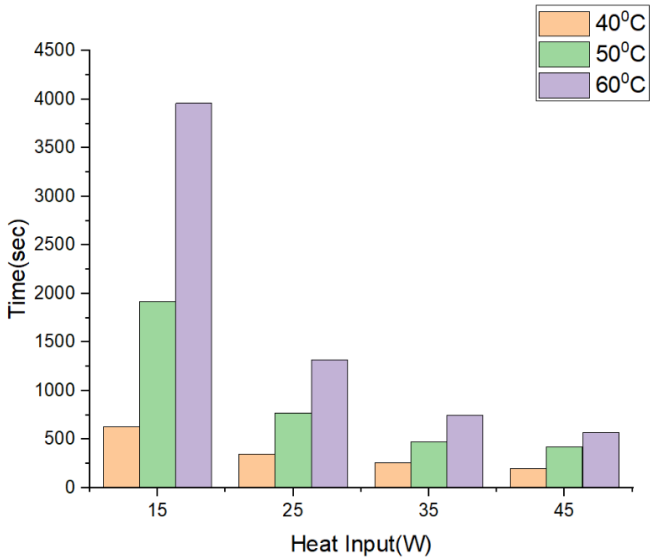

Figure 12. Time taken during heating of CNT-coated heat sink

The time required for the CNT-coated heat sink to reach 40 ^{o}C, 50 ^{o}C, and 60 ^{o}C is displayed in Fig. 12. The heat sink was warmed using 15 W, 25 W, 35 W, and 45 W of input energy. The time needed to reach the maximum temperature was lengthened when the heat input was 15 W. In roughly 690 seconds, the heat sink warmed up to 40 ^{o}C. In the 1980s, the heat sink warmed up to 50 ^{o}C. The heat sink reached 60 ^{o}C at about the same time (about 4000 s). These numbers are all in line with a 15 W heat source. It took longer for the CNT-coated heat sink to reach each of the three temperatures

than the non-coated heat sink. The presence of the CNT covering likely impeded convection with the ambient atmosphere inside the container. Graphene-coated thermal ink exhibited the same behaviour. At maximum temperatures of 40 °C, 50 °C, and 60 °C, increasing the input energy to 25 W decreased the time it took to reach the maximum temperature by 56.5%, 59.6%, and 63.8%. When the highest temperature was 60 ^{o}C, there was a significant drop in the temperature's variability. Adding more energy to the heat sink is assumed to have increased the heat transfer rate via conduction. As a result of this event, heat energy was transferred to the aluminium heat sink rapidly. This phenomenon is explained by the shorter time it takes for the heat sink to reach its maximum temperature when subjected to heat inputs of 35 W and 45 W. Experiments have shown that adding 11% less heat to an aluminium heat sink with the right amount of ceramic particles [28, 29].

3.3. Enhancement ratio of the heat sinks

When the coated heat sinks were heated to a maximum of 40 ^{o}C, as shown in Fig. 13, their enhancement ratio was as high as 1. The percentage of enhancement to heat input increased in the graphene-coated heat sink. The enhancement ratio was slightly enhanced but identical when the heat supply was raised from 35 W to 45 W. The CNT-coated heat sink's ability to dissipate heat at its surface is responsible for this effect. However, when only 15 watts of power were applied, the CNT-coated heat sink showed a significant improvement. However, the enhancement ratio dropped dramatically when the input power was increased to 25 W. The increased input energy likely caused the carbon coating to distribute heat inequitably. Because of this, heat transfer occurred in an uneven condition that needed time to stabilise. The heat sink reached a stable state after some time. The enhancement ratio was slightly enhanced and identical when the heat supply was raised from 35 W to 45 W. The CNT-coated heat sink's ability to dissipate heat at its surface is responsible for this effect.

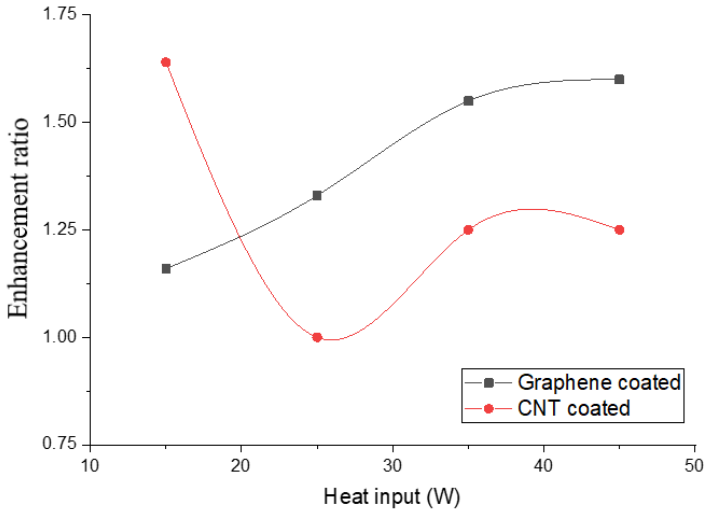

Figure 13. Enhancement ratio at 40 °C

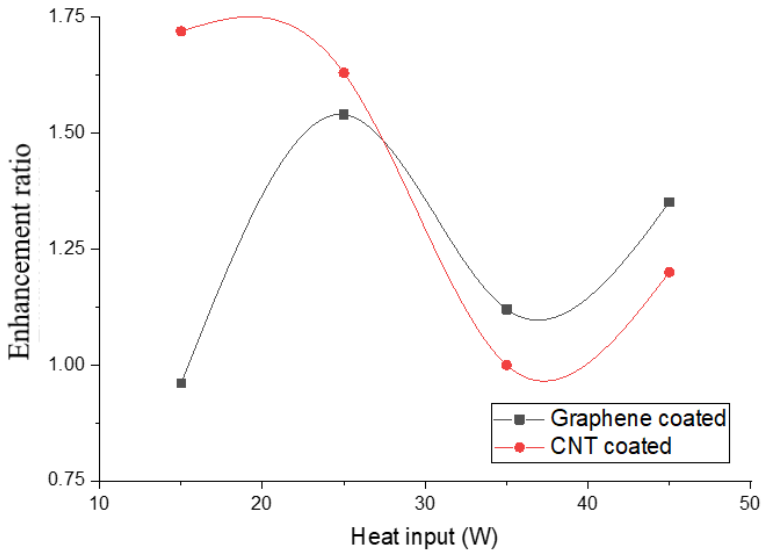

Figure 14. Enhancement ratio at 50 °C

Figure 14 represents the enhancement ratio of the coated heat sinks when they reached a maximum temperature of 50 °C. As the heat input was changed from 15 W to 45 W, the enhancement ratio went from high to low. The enhancement ratio peaked at 25 W of input power. With a 25 W heat input, the graphene coating is inferred to have allowed for adequate heat dissipation. However, as heat input was increased further, heat retention occurred, and the enhancement ratio dropped. The maximum enhancement ratio for CNT coating was achieved at 15 W heat input and then decreased somewhat at 25 W. The enhancement ratio decreased as the heat input was increased further. At both 35 and 45 W input, the enhancement ratio changed in lockstep with the graphene-coated heat sink. This phenomenon supports the hypothesis that elevated heat input produces high heat retention.

In Fig. 15, an enhancement ratio represents the highest temperature the covered heat sinks could reach. The improvement ratio for the coated heat sink was more significant than 1. This demonstrates that the coated heat sinks were successful in transferring heat. Because of this phenomenon, the heat sink's surface temperature rose rapidly, which is helpful. Because of this, the heat sinks were able to improve their convection. When increasing the heat input from 25 W to 40 W, the graphene-coated heat sink maintained an enhancement ratio of roughly 1.15. It was discovered that 15 W was the optimal input power for the CNT, yielding an enhancement ratio of 1.9. The enhancement ratio of the CNT-covered heat sink was observed to drop dramatically with an increase in input energy. The CNT coating's conductivity probably dropped along with the temperature rise. The CNT-coated heat sink provided the lowest enhancement ratio of 1.13 when the input power was 45 W. According to the enhancement ratio calculated for the heat sinks, the CNT coating failed to transfer thermal energy under conditions of rapid heat generation efficiently. On the other hand, the graphene-coated heat sink performed just as well under identical conditions. Experiments showed that applying a metal coating to an aluminium heat sink may increase the heat transfer rate by up to 26% [30].

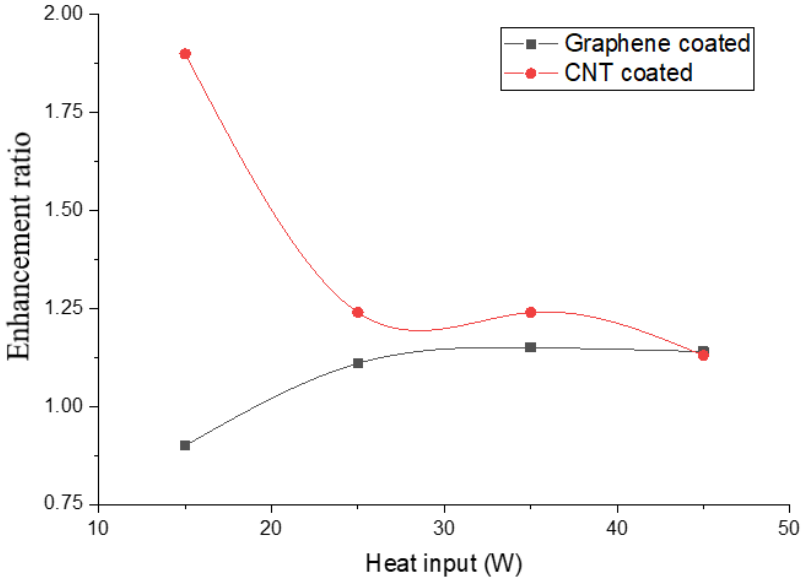

Figure 15. Enhancement ratio at 60 °C

4. Conclusion

A heat sink equipped with side fins was the subject of an experimental study. Graphene and carbon nanotube coatings were developed for use on heat sinks. The heating and cooling cycles were calculated by recording the heat sink's temperature fluctuations and comparing them to those of a non-coated heat sink. Coated heat sinks failed to perform as well as uncoated ones when the input power was low (about 15 W). However, its effectiveness was enhanced by input energies more significant than 15 W. The coated heat sinks reached their maximum temperature of 60 °C rather rapidly as a result. At maximum temperatures of 40 °C, 50 °C, and 60 °C, increasing the input energy to 25 W decreased the time it took to reach the maximum temperature by 56.5%, 59.6%, and 63.8%. Coated heat sinks' heat-conducting capacity was higher than that of non-coated heat sinks when their enhancement ratios were calculated. At various levels of heat application, this phenomenon showed distinct variations. With 15 W of input heat, the CNT-coated heat sink achieved an impressive enhancement ratio of 1.9. However, the graphene-coated heat sinks consistently produced the highest enhancement ratio for 25 W, 35 W, and 45 W of heat input.

References

[1] Wu, Y., et al., Experimental investigation of a PCM-HP heat sink on its thermal performance and anti-thermal-shock capacity for high-power LEDs, *Applied Thermal Engineering, 108* (2016), 5, pp. 192-203

[2] Baby, R., Balaji, C., Thermal performance of a PCM heat sink under different heat loads: an experimental study, *International Journal of Thermal Sciences, 79* (2014), pp. 240-249

[3] Lin, Z., et al., Parametric effect of the interrupted annular groove fin on flow and heat transfer characteristics of a finned circular tube heat exchanger, *Thermal Science, 26* (2022), 6A, pp. 4503-17

[4] Sahoo, S.K., et al., Application of TCE-PCM based heat sinks for cooling of electronic components: A review, *Renewable and Sustainable Energy Reviews, 59* (2016), pp. 550-82

[5] Zheng, D., et al., Heat transfer performance and friction factor of various nanofluids in a double-tube counter flow heat exchanger, Thermal Science, 24 (2020), 6A, pp. 3601-12

[6] Rao, Z, and Wang, S., A review of power battery thermal energy management, *Renewable and Sustainable Energy Reviews*, 15 (2011), pp. 4554-71.

[7] Feng, S., *et al*., Natural convection in a cross-fin heat sink, *Applied Thermal Engineering, 132* (2018), pp. 30-37.

[8] Wang, D., *et al*., Numerical study of the laminar natural convection heat transfer from three attached horizontal isothermal cylinders, *Thermal Science, 26* (2022), 6A, pp. 4797-808.

[9] Fan, A., *et al*., An innovative passive cooling method for high-performance light-emitting diodes, *In 2012 28th Annual IEEE Semiconductor Thermal Measurement and Management Symposium (SEMI-THERM)*, 2012, pp. 319-324.

[10] Pongiannan, S.K., *et al*., Natural-convection heat transfer enhancement of aluminium heat sink using nanocoating by electron beam method, *Thermal Science, 23* (2019), 5B, pp. 3129-41.

[11] Habib, N., and Tahir. M., Thermal analysis of proposed heat sink design under natural convection for the thermal management of electronics, *Thermal Science, 26* (2022), 2, pp. 1487-501.

[12] Jia, Y., *et al*., Heat transfer and fluid flow characteristics of microchannel with oval-shaped micro pin fins, *Entropy, 23* (2021), 11, 1482.

[13] Baig, T., *et al*., Thermal performance investigation of slotted fin minichannel heat sink for microprocessor cooling, *Energies,14* (2021), 19, 6347.

[14] Jasim, H.A., *et al.*, Investigation of heat transfer enhancement for different shapes pin-fin heatsink. *J Mech Eng Res Dev, 44* (2021), 3, pp. 75-89.

[15] Wang, H, *et al*., Heat transfer performance of a novel tubular oscillating heat pipe with sintered copper particles inside flat-plate evaporator and high-power LED heat sink application, *Energy Conversion and Management, 189* (2019), pp. 215-22.

[16] Ali *et al*., Thermal management of electronics: An experimental analysis of triangular, rectangular and circular pin-fin heat sinks for various PCMs, *International Journal of Heat and Mass Transfer, 123* (2018), pp. 272-84.

[17] Mukesh Kumar, P.C., and Kumar, A., Influence of aspect ratio on thermal performance of heat sink using ansys, *Journal of Applied Fluid Mechanics, 11* (2018), pp. 45-52.

[18] Senthilkumar, R., *et al*., Experimental investigation on carbon nano tubes coated brass rectangular extended surfaces, *Applied Thermal Engineering, 50* (2013), 1, pp. 1361-1368.

[19] Zou, D., *et al*., Thermal performance enhancement of composite phase change materials (PCM) using graphene and carbon nanotubes as additives for the potential application in lithium-ion power battery, *International Journal of Heat and Mass Transfer, 120* (2018), pp. 33-41.

[20] Mahmoud, S., *et al*., Experimental investigation of inserts configurations and PCM type on the thermal performance of PCM based heat sinks, *Applied Energy, 112* (2013), pp. 1349-56.

[21] Prakash, D.S., and Raja, N.D., Investigation of tribological behavior and the mechanical properties of TiB2, Al2O3 reinforced AA6061 matrix sintered hybrid composites, *Iran. J. Mater. Sci. Eng., 18* (2021), 4, pp. 1-3.

[22] Verma *et al*., Multiwalled Carbon Nanotube-Poly Vinyl Alcohol Nanocomposite Multifunctional Coatings on Aerospace Alloys, *Materials Today: Proceedings, 5* (2018), 10, pp. 21205–21216.

[23] Moffat, R.J., Describing the uncertainties in experimental results, Experimental *Thermal and Fluid Science*, 1 (1988), 1, pp. 3-17.

[24] Madhaiyan, R. *et al*., Experimental study on heat transfer performance of variable area straight fin heat sinks with PCM, *Thermal Science*, *26* (2022), 2A, pp. 983-989.

[25] Kuang, H., *et al*., Wettability and thermal contact resistance of thermal interface material composited by gallium-based liquid metal on copper foam, *International Journal of Heat and Mass Transfer*, *199* (2022), 123444.

[26] Zu, H., *et al*., Analysis of enhanced heat transfer on a passive heat sink with high-emissivity coating, *International Journal of Thermal Sciences*, *166* (2021), 106971.

[27] Arulprakasajothi, M., *et al*., Experimental investigation of salinity gradient solar pond with nano-based phase change materials, *Energy Sources, Part A: Recovery, Utilization, and Environmental Effects*, *45* (2023), 2, pp. 5465-80.

[28] Tsai, W.Y., *et al*., High thermal dissipation of Al heat sink when inserting ceramic powders by ultrasonic mechanical coating and armoring, *Materials*, *10* (2017), 5, 454.

[29] Muthu, G., *et al*., Performance of solar parabolic dish thermoelectric generator with PCM, *Materials Today: Proceedings*, *37* (2021), pp. 929-33.

[30] Li, X., *et al*., Parametric study on heat transfer and pressure drop of twisted oval tube bundle with inline layout, *International Journal of Heat and Mass Transfer*, *135* (2019), pp. 860-872.

Submitted: 15.07.2023.

Revised: 14.09.2023.

Accepted: 21.09.2023.